APPLIED GEOPHYSICS, Vol.13, No.1 (March 2016), P. 13-24, 12 Figures.
DOI:10.1007/s11770-016-0530-8

Two-dimensional inversion of spectral induced polarization data using MPI parallel algorithm in data space*

Zhang Zhi-Yong[1,2],Tan Han-Dong♦[1,2], Wang Kun-Peng[1,2], Lin Chang-Hong[1,2], Zhang Bin[3], and Xie Mao-Bi[1,2]

Abstract: Traditional two-dimensional (2D) complex resistivity forward modeling is based on Poisson's equation but spectral induced polarization (SIP) data are the coproducts of the induced polarization (IP) and the electromagnetic induction (EMI) effects. This is especially true under high frequencies, where the EMI effect can exceed the IP effect. 2D inversion that only considers the IP effect reduces the reliability of the inversion data. In this paper, we derive differential equations using Maxwell's equations. With the introduction of the Cole–Cole model, we use the finite-element method to conduct 2D SIP forward modeling that considers the EMI and IP effects simultaneously. The data-space Occam method, in which different constraints to the model smoothness and parametric boundaries are introduced, is then used to simultaneously obtain the four parameters of the Cole–Cole model using multi-array electric field data. This approach not only improves the stability of the inversion but also significantly reduces the solution ambiguity. To improve the computational efficiency, message passing interface programming was used to accelerate the 2D SIP forward modeling and inversion. Synthetic datasets were tested using both serial and parallel algorithms, and the tests suggest that the proposed parallel algorithm is robust and efficient.
Keywords: Spectral induced polarization, 2D inversion, data-space method, Cole–Cole model, MPI parallel computation

Introduction

The spectral induced polarization (SIP) method, also called the complex resistivity method, is an induced polarization (IP) method that is based on the frequency spectrum or the time spectrum, difference in rock resistivity, and is used to investigate geological anomalies by measuring the apparent complex resistivity spectrum or the time-varying resistivity spectrum.

Manuscript received by the Editor November 22, 2015; revised manuscript received February 14, 2016.
*This work is jointly sponsored by the National Natural Science Foundation of China (Grant No. 41374078) , the Geological Survey Projects of the Ministry of Land and Resources of China (Grant Nos. 12120113086100 and 12120113101300), and Beijing Higher Education Young Elite Teacher Project.
1. School of Geophysics and Information Technology, China University of Geosciences, Beijing 100083, China.
2. Key Laboratory of Geo-detection (China University of Geosciences, Beijing), Ministry of Education, Beijing 100083, China.
3. China Non-ferrous Metals Resource Geological Survey, Beijing 100012, China.
♦Corresponding author: Tan Han-Dong (thd@cugb.edu.cn)

Based on the spectral parameters and the evaluation of electrical abnormalities in rocks, geological problems can be solved (Yang, 2011). Compared with other geophysical methods, the SIP method uses the rock electrochemistry to obtain multiple subsurface parameters simultaneously. Through the comparison and interpretation of these parameters, large amounts of geoelectrical data are produced. Presently, the SIP method is used in mining exploration (Shin et al., 2015), hydrogeology (Revil et al., 2012; Attwa and Günther, 2013), environmental monitoring (Kemna et al., 2000), and monitoring the organic pollution in rocks and soils (Schwartz and Furman, 2012).

Loke et al. (2006) used the Poisson equation to carry out forward modeling without considering the EMI effect. They used a nonhomogeneous initial model, which is obtained from an approximate inversion, to successfully invert a 2D SIP synthetic dataset. Presently, the forward modeling and inversion of the SIP method, which is based on Maxwell's equations, are actively researched in applied geophysics. Xu (2007) performed 2D SIP forward modeling using the finite-element method and used the damped least squares method to perform the inversion . Zhao (2009) used the damped least squares method to perform 2D SIP inversion in the presence of topography. Fan et al. (2012) added Occam' s algorithm as a model constraint to the least squares objective function in 2.5D SIP inversion.

The finite-element method (FEM) is well suited for handling complex boundaries and geometries (Avdeev, 2005), and satisfies the requirements for accuracy and speed in 2D SIP forward modeling. In the inversion, the damped least squares method only considers data fitting and does not constrain the model. In this study, we apply the data-space Occam (DASOCC) inversion method (Siripunvaraporn et al., 2000) to 2D SIP inversion. The approach is a variant of the Occam inversion method (Constable et al., 1987) and uses the principle of fitting observations by the smoothest model. The Lagrange multiplier λ is obtained using this inversion method, requiring only a small number of iterations to converge. In this study, we invert the four parameters of the Cole –Cole model simultaneously. The model parameters (M) outnumber the observed data points (N), leading to serious undetermined problems. Thus, we adopt the strategy of using different constraints to enhance model smoothness and to limit parametric boundaries to significantly reduce ambiguity and improve the stability of the inversion. After using a serial algorithm, we introduce the message passing interface (MPI) (Pacheco, 2011) to conduct forward modeling and inversion based on the SIP method. The results and efficiency are then tested against the simulated data.

Forward modeling

The classical approach to CR forward modeling uses the complex resistivity defined by the Cole–Cole model (Pelton et al., 1978) to replace the ground resistivity. Experimental studies (Pelton et al., 1978) have shown that the complex resistivity spectrum of the uniform dielectric can be represented by the Cole–Cole model

$$\rho(i\omega) = \rho_0 \left\{ 1 - m \left[1 - \frac{1}{1 + (i\omega\tau)^c} \right] \right\}, \qquad (1)$$

where $\rho(i\omega)$ is the complex resistivity; ρ_0 is the DC resistivity and ranges from 10^{-4} Ω·m to 10^6 Ω·m; c is the relaxation constant and is between 0.1 and 0.6, and denotes the particle-distribution pattern; τ is the time constant with range from 10^{-3} s to 5×10^{-3} s and denotes the average size distribution of the IP targets; m is the chargeability, it is between 0.1 to 0.98, and denotes the IP effect (Fan, 2013; Routh et al., 1998). The resistivity referred to below is the complex resistivity of equation (1).

2D FEM modeling

The 2D earth model considered in this study is shown in Figure 1. The strike is the y-direction. The resistivity is constant in the y-direction and only varies in the xz-plane.

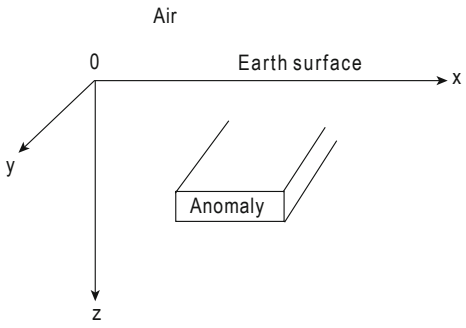

Fig.1 Two-dimensional geoelectrical model.

Assuming the time dependence is e^{iwt} and neglecting the effect of the displacement current, we can use Maxwell's equations to obtain the secondary electric field

$$\nabla \times \mathbf{E}^s = -i\omega\mu_0 \mathbf{H}^s, \qquad (2)$$

$$\nabla \times \mathbf{H}^s = \sigma \mathbf{E}^s + \sigma_a \mathbf{E}^p, \tag{3}$$

where **E** is the electric field and **H** is the magnetic field, and superscripts *p* and *s* denote the primary and secondary field, respectively, $i = \sqrt{-1}$, $\omega = 2\pi f$ is the angular frequency, μ_0 is the magnetic permeability in free space, σ is the complex conductivity, and the anomalous complex conductivity is $\sigma_a = \sigma - \sigma_0$.

Using the Fourier transform, equations (2) and (3) can be transformed with respect to the strike direction, and the data can be analyzed in the wavenumber domain (x, k_y, z). The application of the FEM (Zienkiewicz, 1977) to the above equations produces the following equations (Mitsuhata, 2000)

$$\begin{aligned}
&\sum_{e=1}^{N_e} \iint_{D_e} \{\frac{\partial N_i^e}{\partial x}(\frac{\hat{y}}{k_e^2}\cdot\frac{\partial \hat{E}_y^s}{\partial x}) + \frac{\partial N_i^e}{\partial z}(\frac{\hat{y}}{k_e^2}\cdot\frac{\partial \hat{E}_y^s}{\partial z}) + N_i^e \hat{y}\hat{E}_y^s \\
&+ \frac{ik_y}{k_e^2}(\frac{\partial N_i^e}{\partial x}\cdot\frac{\partial \hat{H}_y^s}{\partial z} - \frac{\partial N_i^e}{\partial z}\cdot\frac{\partial \hat{H}_y^s}{\partial x})\}dxdz \\
&= -\sum_{e=1}^{N_e} \iint_{D_e} \{N_i \sigma_a \hat{E}_y^p + \frac{ik_y\sigma_a}{k_e^2}(\frac{\partial N_i}{\partial x}\hat{E}_x^p + \frac{\partial N_i}{\partial z}\hat{E}_z^p)\}dxdz,
\end{aligned} \tag{4}$$

$$\begin{aligned}
&\sum_{e=1}^{N_e} \iint_{D_e} \{\frac{\partial N_i^e}{\partial x}(\frac{\hat{z}}{k_e^2}\cdot\frac{\partial \hat{H}_y^s}{\partial x}) + \frac{\partial N_i^e}{\partial z}(\frac{\hat{z}}{k_e^2}\cdot\frac{\partial \hat{H}_y^s}{\partial z}) + N_i^e \hat{z}\hat{H}_y^s \\
&+ \frac{ik_y}{k_e^2}(-\frac{\partial N_i^e}{\partial x}\cdot\frac{\partial \hat{E}_y^s}{\partial z} + \frac{\partial N_i^e}{\partial z}\cdot\frac{\partial \hat{E}_y^s}{\partial x})\}dxdz \\
&= -\sum_{e=1}^{N_e} \iint_{D_e} \{\frac{\hat{z}\sigma_a}{k_e^2}(\frac{\partial N_i}{\partial x}\hat{E}_x^p - \frac{\partial N_i}{\partial z}\hat{E}_z^p)\}dxdz,
\end{aligned} \tag{5}$$

where "^" denotes the quantity in the wavenumber domain, N_e is the number of subdivided rectangular finite elements, N_i^e is the interpolation function of the ith node in the eth element, $k_e^2 = k_y^2 - k^2$ and $k^2 = -\hat{z}\hat{y}$, the impedivity $\hat{z} = i\mu\omega$, the admittivity $\hat{y} = \sigma$, the wavenumber along strike is k_y, $\hat{E}_x^p$, $\hat{E}_y^p$, and $\hat{E}_z^p$ correspond to the primary electric field components in the x-, y-, and z-directions in the wavenumber domain, and $\hat{E}_y^s$ and $\hat{H}_y^s$ correspond to the secondary electric and magnetic field parameters along strike (y-axis) in the wavenumber domain.

To solve equations (4) and (5), we need to obtain the primary electric field of the underground grid nodes in the wavenumber domain. Based on electromagnetic theory (Nabighian, 1988), we derive the equation for the electric field component generated by the horizontal electrical dipole in the x-direction as follows:

$$\begin{cases}
\hat{E}_x(x,k_y,z) = -\frac{1}{\pi}\int_0^\infty [\frac{u_1 k_x^2}{\hat{y}} + \frac{\hat{z}k_y^2}{u_0+u_1}]\frac{e^{-u_1 z}}{k_x^2+k_y^2}\cos(k_x x)dkx \\
\hat{E}_y(x,k_y,z) = -\frac{i}{\pi}\int_0^\infty [\frac{u_1}{\hat{y}} - \frac{\hat{z}}{u_0+u_1}]\frac{k_x k_y e^{-u_1 z}}{k_x^2+k_y^2}\sin(k_x x)dkx, \\
\hat{E}_z(x,k_y,z) = \frac{1}{\pi}\int_0^\infty \frac{k_x}{\hat{y}} e^{-u_1 z}\sin(k_x x)dkx
\end{cases} \tag{6}$$

where

$$u_0 = \sqrt{k_x^2 + k_y^2 - (-i\omega\mu_0\sigma_{air})}, \quad u_1 = \sqrt{k_x^2 + k_y^2 - (-i\omega\mu_0\sigma)},$$

and σ_{air} is the conductivity of *air*.

In equation for the secondary electric field along the x-axis, $\hat{E}_x^s$ in the wavenumber domain (Li and Key, 2007) is

$$\hat{E}_x^s = q\frac{\partial \hat{E}_y^s}{\partial x} + p\frac{\partial \hat{H}_y^s}{\partial z} + p\sigma_a \hat{E}_x^p, \tag{7}$$

where $p = \frac{i\omega\mu_0}{k^2 - k_y^2}$, $q = \frac{ik_y}{k^2 - k_y^2}$, and $k^2 = -i\omega\mu_0\sigma$.

$\hat{E}_x^s$ is added to $\hat{E}_x^p$ to obtain the total electric field $\hat{E}_x$. Then, E_x can be obtained by the inverse Fourier transformation of $\hat{E}_x$ and the forward modeling is complete.

Validation of the 2D program

To validate the 2D SIP forward modeling algorithm, we designed a 2D model, as shown in Figure 2. The horizontal electric dipole source is at the origin ($x = y = z = 0$) and its dipole moment is 1 A·m. There are 25 receivers from x = 0 m to x =1000 m. The horizontal electric field is calculated at frequencies of 32 Hz and 128 Hz.

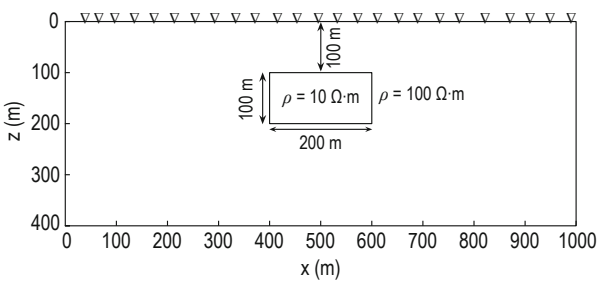

Fig.2 The 2D model.

We use the 2.5D CSEM program of Key and Ovall (2011) and our finite element program to calculate the

forward response and obtain the horizontal electric field E_x, respectively. The 2D model has eleven air layers and is divided into 113 × 64 discrete blocks in the xz-plane. The background resistivity is 100 Ω·m. The results for the total electric field calculated with both programs are shown in Figure 3. The results are almost identical, which indicates that the 2D program is correct.

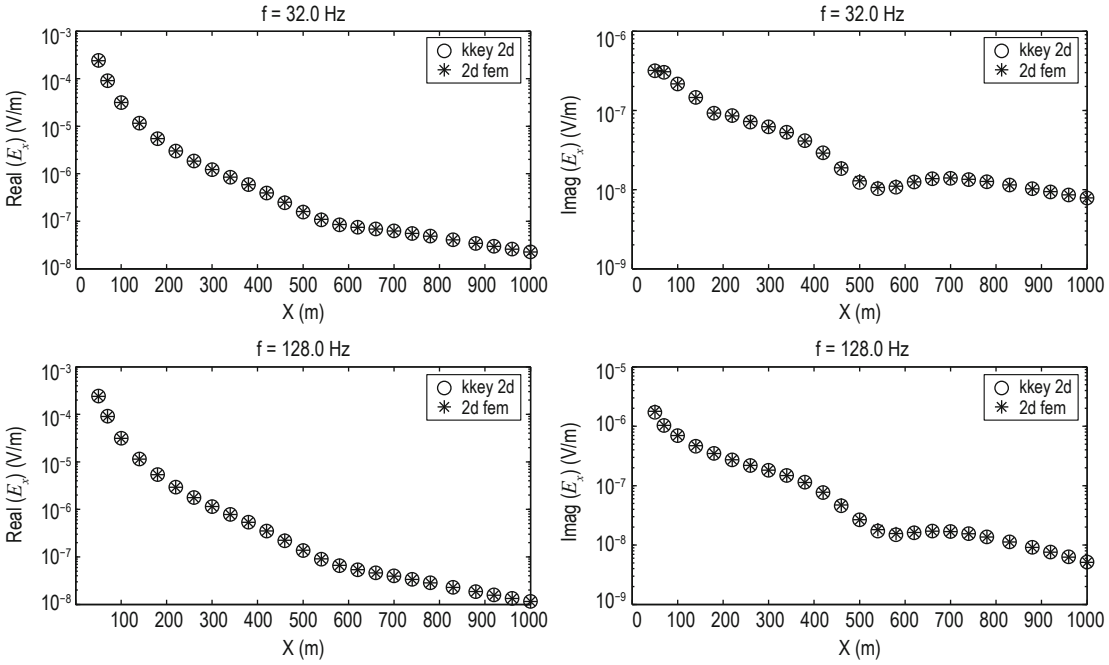

Fig.3 The E_x response comparison between the 2D finite element modeling results and the results generated from 2.5DCSEM.

Inversion

Data-space method

The data-space Occam method was successfully applied to 2D and 3D magnetotelluric (MT) inversion (Siripunvaraporn and Egbert, 2000; Siripunvaraporn et al., 2005). The method transforms the calculation and storage of model space (M × M) to the calculation and storage of the model data space (N × N). Generally, the fact that the number of data points (N) is less than the number of models reduces the dimensions of the system equations and requirements. The data-space Occam method follows Occam's principle and finds the smoothest model to fit the observed data. Mathematically, this can be transformed to find the minimum of the unconstrained function $U(\mathbf{m}, \lambda)$

$$U(\mathbf{m},\lambda) = (\mathbf{m}-\mathbf{m}_0)^{\mathrm{T}}\mathbf{C}_{\mathbf{m}}^{-1}(\mathbf{m}-\mathbf{m}_0) + \lambda^{-1}\left\{(\mathbf{d}-\mathbf{F}[\mathbf{m}])^{\mathrm{T}}\mathbf{C}_{\mathbf{d}}^{-1}(\mathbf{d}-\mathbf{F}[\mathbf{m}]) - X_*^2\right\}, \quad (8)$$

where $\mathbf{m}=[m_1, m_2, \ldots, m_{4M}]$ is the vector of the model, $\mathbf{m}_0$ is the prior model, $\mathbf{C}_m$ is the model covariance matrix, $\mathbf{C}_d$ is the data covariance matrix, $\mathbf{d}=[d_1, d_2, \ldots, d_N]$ is the vector of the observed data, $\mathbf{F}(\mathbf{m})$ is the model response, λ is the Lagrange multiplier, X_*^2 is the desired level of misfit, and subscript T denotes the matrix transposition.

It is not straightforward to find the stationary points of U because it is a function of m and λ. In Occam's method, the minimum of λ is sought automatically and for a given λ, equation (8) is transformed to the objective function $W_\lambda(\mathbf{m})$

$$W_\lambda(\mathbf{m}) = (\mathbf{m}-\mathbf{m}_0)^{\mathrm{T}}\mathbf{C}_{\mathbf{m}}^{-1}(\mathbf{m}-\mathbf{m}_0) + \lambda^{-1}\left\{(\mathbf{d}-\mathbf{F}[\mathbf{m}])^{\mathrm{T}}\mathbf{C}_{\mathbf{d}}^{-1}(\mathbf{d}-\mathbf{F}[\mathbf{m}])\right\}. \quad (9)$$

Inversion is a nonlinear problem and we need to transform this nonlinearity by linearizing $\mathbf{F}(\mathbf{m})$ as a Taylor series expansion

$$\mathbf{F}[\mathbf{m}_{k+1}] = \mathbf{F}[\mathbf{m}_k + \Delta\mathbf{m}] = \mathbf{F}[\mathbf{m}_k] + \mathbf{J}_k(\mathbf{m}_{k+1} - \mathbf{m}_k), \quad (10)$$

where $\mathbf{J}_k = (\partial\mathbf{F}/\partial\mathbf{m})_{m_k}$ is the N × 4M sensitivity matrix

calculated at m_k. We substitute equation (10) into (9) and we obtain

$$W_\lambda(\mathbf{m}_{k+1}) = (\mathbf{m}_{k+1}-\mathbf{m}_0)^{\mathrm{T}}\mathbf{C}_{\mathbf{m}}^{-1}(\mathbf{m}_{k+1}-\mathbf{m}_0) + \lambda^{-1}\left\{\begin{array}{l}\left(\mathbf{d}-\mathbf{F}[\mathbf{m}_k]-\mathbf{J}_k\mathbf{m}_{k+1}+\mathbf{J}_k\mathbf{m}_k\right)^{\mathrm{T}} \\ \cdot\mathbf{C}_{\mathbf{d}}^{-1}\left(\mathbf{d}-\mathbf{F}[\mathbf{m}_k]-\mathbf{J}_k\mathbf{m}_{k+1}+\mathbf{J}_k\mathbf{m}_k\right)\end{array}\right\}. \quad (11)$$

The problem then becomes finding the minimum of equation (11), which is a quadratic function of m. Differentiating equation (11) with respect to the model parameter m and setting it to zero, we obtain iteratively approximate solutions in the model domain

$$\mathbf{m}_{k+1}-\mathbf{m}_0 = [\lambda\mathbf{C}_{\mathbf{m}}^{-1}+\mathbf{\Gamma}_k^{\mathbf{m}}]^{-1}\mathbf{J}_k^{\mathbf{T}}\mathbf{C}_{\mathbf{d}}^{-1}\boldsymbol{\chi}_k, \quad (12)$$

where $\boldsymbol{\chi}_k = \mathbf{d}-\mathbf{F}[\mathbf{m}_k]+\mathbf{J}_k(\mathbf{m}_k-\mathbf{m}_0)$, and $\mathbf{\Gamma}_k^{\mathbf{m}} = \mathbf{J}_k^{\mathrm{T}}\mathbf{C}_{\mathbf{d}}^{-1}\mathbf{J}_k$ is a 4M × 4M positive semidefinite symmetric matrix. The inversion results are obtained by iteratively solving equation (12).

After transforming equation (12), we obtain the iterative approximate solutions in the data-space domain

$$\mathbf{m}_{k+1}-\mathbf{m}_0 = \mathbf{C}_{\mathbf{m}}\mathbf{J}_k^{\mathrm{T}}[\lambda\mathbf{C}_{\mathbf{d}}+\mathbf{\Gamma}_k^{\mathbf{n}}]^{-1}\boldsymbol{\chi}_k, \quad (13)$$

where $\mathbf{\Gamma}_k^n = \mathbf{J}_k\mathbf{C}_{\mathbf{m}}\mathbf{J}_k^{\mathrm{T}}$ is a 4N × 4N positive semidefinite symmetric matrix.

In the SIP data-space Occam's inversion method, the Lagrange multiplier is a vector of different values for the different parameters of the Cole–Cole model. Routh et al. (1998) used the relative difference in the model roughness vectors, chargeability, relaxation constant, and time constant to derive the relative weight of the three parameters. Loke et al. (2006) adopted the chargeability sensitivity matrix norm, the relaxation constant sensitivity matrix norm, and the time constant sensitivity matrix norm as weights for the DC resistivity sensitivity matrix norm. In this study, we use a slightly different method in which the weights of the DC resistivity sensitivity matrix 2-norm are the chargeability sensitivity matrix 2-norm, the relaxation constant sensitivity matrix 2-norm, and the time constant sensitivity matrix 2-norm

$$\frac{\lambda_{\rho_0}}{\lambda_m} = \frac{\sum\left\|\mathbf{J}_{k\rho_0}\right\|_2}{\sum\left\|\mathbf{J}_{km}\right\|_2}, \quad (14)$$

$$\frac{\lambda_{\rho_0}}{\lambda_c} = \frac{\sum\left\|\mathbf{J}_{k\rho_0}\right\|_2}{\sum\left\|\mathbf{J}_{kc}\right\|_2}, \quad (15)$$

$$\frac{\lambda_{\rho_0}}{\lambda_\tau} = \frac{\sum\left\|\mathbf{J}_{k\rho_0}\right\|_2}{\sum\left\|\mathbf{J}_{k\tau}\right\|_2}, \quad (16)$$

where $\lambda_{\rho 0}$, λ_m, λ_c, and λ_τ are the Lagrange multipliers for the DC resistivity, the chargeability, the relaxation constant, and the time constant, respectively, and $\mathbf{J}_{k\rho 0}$, $\mathbf{J}_{km}$, $\mathbf{J}_{kc}$, and $\mathbf{J}_{k\tau}$ are the sensitivity matrices for the DC resistivity, the chargeability, the relaxation constant, and the time constant.

Using equations (12) and (13), we solve the equation with 4M × 4M dimensions in the model space, whereas in the data space we solve the equation in the N × N dimensions. In general, the number of observed data points N is less than that of the models 4M. Thus the data-space inversion requires less calculations, time, and memory than the model-space inversion. Moreover, we calculate the inverse of the model covariance matrix $\mathbf{C}_{\mathbf{m}}^{-1}$ in model space. Generally, it is not practical to calculate the inverse of the full 4M × 4M model covariance matrix. However, there is no calculation of $\mathbf{C}_{\mathbf{m}}^{-1}$ in the data-space Occam algorithm. In this study, we adopt the method of Egbert et al. (1994) to rapidly calculate $\mathbf{C}_{\mathbf{m}}$.

Sensitivity calculation

Adjoint equation method

The adjoint equation method is an effective method to calculate the sensitivity matrix in 2D electromagnetic inversion. McGillivray et al. (1994) introduced the adjoint equation method to the frequency-domain EM problem with good results. Owing to the fact that we use the horizontal electric field E_x, as the observed data in the inversion, the sensitivity matrix equation for electromagnetism can be obtained using the adjoint equation proposed by McGillivray et al. (1994)

$$\int_D(\tilde{\mathbf{M}}_s\cdot\frac{\partial\mathbf{H}}{\partial\sigma_{\mathrm{j}}}+\tilde{\mathbf{J}}_s\cdot\frac{\partial\mathbf{E}}{\partial\sigma_j})dv = \int_D\mathbf{E}^+\cdot\mathbf{E}\,\psi_j(\mathbf{x})dv, \quad (17)$$

where $\tilde{\mathbf{M}}_s$ and $\tilde{\mathbf{J}}_s$ are the magnetic and electric sources, respectively, $\mathbf{E}^+$ is the auxiliary electric field, $\mathbf{E}$ is the electric field, $\psi_k(\mathbf{x})$ is the chosen basis function, D is the finite space domain, and v is the volume element.

The partial derivative of the electric or magnetic field with respect to conductivity is derived by choosing different adjoint sources. For example, to obtain $\partial\mathbf{E}/\partial\sigma_j$ at location x_0, we select the electric source in the x-direction, where $\tilde{\mathbf{J}}_s = \delta(\mathbf{x}-\mathbf{x}_0)\hat{x}$, and the magnetic source $\tilde{\mathbf{M}}_s = 0$. Then, equation (17) becomes

$$\frac{\partial E_x(\mathbf{x}_0)}{\partial \sigma_j} = \int_D \mathbf{E}^+ \cdot \mathbf{E}\psi_j(\mathbf{x})dv, \quad (18)$$

where $\partial E_x(\mathbf{x}_0)/\partial\sigma_j$ is the partial derivative of the electric field E_x with respect to σ_j at the observation location x_0.

To calculate $\partial E_x(\mathbf{x}_0)/\partial\sigma_j$, the electric field $\mathbf{E}$, comprised the grid points generated by the original source in the forward modeling, should be determined. The electric field $\mathbf{E}^+$, comprised the grid points generated by the adjoint source in the forward modeling, should then be calculated. After $\mathbf{E}$ and $\mathbf{E}^+$ are determined, $\partial E_x(\mathbf{x}_0)/\partial\sigma_j$ can be calculated using equation (18).

Sensitivity matrix derivation and calculation

We first calculate $\partial E_x/\partial\sigma_j$ in the wavenumber domain and subsequently use the inverse Fourier transformation to obtain $\partial E_x/\partial\sigma_j$ in the space domain. The electric field component of the underground grid points is calculated in the wavenumber domain. The equation for the sensitivity matrix is derived in the wavenumber domain.

In the two-dimensional problem, conductivity is constant along strike (y). Equation (18) then transforms to

$$\frac{\partial \mathbf{E}_x}{\partial \sigma_j} = \int_{-\infty}^{\infty}\int_{A_j} \mathbf{E}^+ \cdot \mathbf{E}dsdy. \quad (19)$$

The electric field $\mathbf{E}$ in the frequency domain can be obtained using the inverse Fourier transformation of $\hat{\mathbf{E}}$

$$\mathbf{E}(x,y,z) = \frac{1}{2\pi}\int_{-\infty}^{\infty} \hat{\mathbf{E}}(x,k_y,z)e^{ik_y y}dk_y. \quad (20)$$

Similarly, the adjoint electric field can be represented as

$$\mathbf{E}^+(x,y,z) = \frac{1}{2\pi}\int_{-\infty}^{\infty} \hat{\mathbf{E}}^+(x,k_y',z)e^{ik_y' y}dk_y'. \quad (21)$$

Substituting equations (20) and (21) into equation (19)

$$\frac{\partial \mathbf{E}_x}{\partial \sigma_j} = \frac{1}{4\pi^2}\int_{-\infty}^{\infty}\int_{-\infty}^{\infty}\int_{-\infty}^{\infty} \hat{\mathbf{A}}(k_y,k_y')e^{i(k_y+k_y')y}dk_y dk_y' dy. \quad (22)$$

$\hat{\mathbf{A}}$ is defined as

$$\hat{\mathbf{A}}(k_y,k_y') = \int_{A_j} \hat{\mathbf{E}}(x,k_y,z)\cdot\hat{\mathbf{E}}^+(x,k_y',z)ds. \quad (23)$$

Using the Dirac delta function

$$\delta(k_y) = \frac{1}{2\pi}\int_{-\infty}^{\infty} e^{ik_y y}dy. \quad (24)$$

Equation (19) transforms

$$\frac{\partial \mathbf{E}_x}{\partial \sigma_j} = \frac{1}{2\pi}\int_{-\infty}^{\infty}\int_{-\infty}^{\infty} \hat{\mathbf{A}}(k_y,k_y')\delta(k_y+k_y')dk_y dk_y'. \quad (25)$$

Utilizing the sifting property of the Dirac delta function:

$$\int_{-\infty}^{\infty}\delta(t-t_0)f(t)dt = f(t_0). \quad (26)$$

Then, equation (25) becomes

$$\frac{\partial \mathbf{E}_x}{\partial \sigma_j} = \frac{1}{2\pi}\int_{-\infty}^{\infty} \hat{\mathbf{A}}(k_y,-k_y)dk_y. \quad (27)$$

For a horizontal electric dipole, $\hat{\mathbf{E}}_x$, $\hat{\mathbf{E}}_y$, and $\hat{\mathbf{E}}_z$ are the electric field components in the wavenumber domain generated by the original source, and $\hat{\mathbf{E}}_x^+$, $\hat{\mathbf{E}}_y^+$, and $\hat{\mathbf{E}}_z^+$ are the electric field components in the wavenumber domain generated by the adjoint source. From equation (6), it can be seen that $\hat{\mathbf{E}}_x$, $\hat{\mathbf{E}}_x^+$, $\hat{\mathbf{E}}_z$, and $\hat{\mathbf{E}}_z^+$ are even functions of k_y, whereas $\hat{\mathbf{E}}_y$ and $\hat{\mathbf{E}}_y^+$ are odd functions of k_y. Then, according to the parity of the electric field components, we obtain the sensitivity matrix equation

$$\frac{\partial \mathbf{E}_x}{\partial \sigma_j} = \frac{1}{\pi}\int_0^{\infty}\int_{A_j}(\hat{\mathbf{E}}_x\cdot\hat{\mathbf{E}}_x^+ - \hat{\mathbf{E}}_y\cdot\hat{\mathbf{E}}_y^+ + \hat{\mathbf{E}}_z\cdot\hat{\mathbf{E}}_z^+)dsdk_y. \quad (28)$$

Constraining the model parameters

The inversion of the four parameters of the Cole–Cole model increases the nonuniqueness of the inversion; thus, the problem is constraining the model parameters. The introduction of model parameter constraints reduces the nonuniqueness and avoids estimating nonphysical parameters in the inversion. We use a simple constraint (Kim et al., 1999; Commer and Newman, 2008) to constrain the Cole–Cole model parameters. We define a new vector x, as the vector of the inversion solution that is related to the model parameter $\mathbf{m}$ as follows:

$$m_j = \frac{a_j + b_j\exp(x_j)}{1+\exp(x_j)}; \quad -\infty < x_j < \infty, \quad (29)$$

$$x_j = \log(m_j - a_j) - \log(b_j - m_j); \quad a_j < m_j < b_j, \quad (30)$$

$$\frac{\partial m_j}{\partial x_j} = \frac{(b_j - a_j)\exp(x_j)}{\left[1+\exp(x_j)\right]^2}, \quad (31)$$

where a_j and b_j is the minimum and maximum of

the jth model parameter respectively, m_j is the jth model parameter, x_j is the jth model parameter after transformation, and exp is the natural exponential function.

The partial derivative of the electric field component E_x with respect to the constraint parameter vector x can be obtained using the sensitivity matrix

$$\frac{\partial \mathbf{E}_x}{\partial x_j} = -\frac{1}{\left(\rho_j\right)^2}\frac{\partial \mathbf{E}_x}{\partial \sigma_j}\frac{\partial \rho_j}{\partial m_j}\frac{\partial m_j}{\partial x_j}, \quad (32)$$

where ρ_j is the complex resistivity of the jth element, and σ_j is the complex conductivity of the jth element.

We use synthetic multi-array electric field data in the inversion and we examine the difference between multi- and single-array electric data as a function of the number of observations and dimension size off the sensitivity matrix.

MPI parallel programming

2D SIP inversion is time consuming, as it includes the calculation of the primary electric field generated by the adjoint source in the wavenumber domain, forward modeling, and the sensitivity matrix calculation. It is therefore sensible to apply parallel algorithms to calculate these parameters. More, after analyzing the serial algorithm, it was found that the primary electric field, and the sensitivity matrix and forward modeling represent different transmitting sources and are independent of each other.

In MPI parallel programming, there is the equal pattern and the principal-subordinate pattern design. We adopt the principal-subordinate pattern, which consists of the main process and the subroutine process. The main process maintains the global data structure, the distribution of the parameter information, the assignment of tasks, sending the parameters, assembling the calculated results from other processes, and outputting the final result. The subroutine process accepts the parameters from the main process, executes the calculation of the assigned tasks from the main process, and sends the results to the main process. The parallel computation framework is shown in Figure 4. Its basic principles are the initialization of the parallel environment, and the reading of the parameter information from the main process and their distribution to the other processes. According to the assigned tasks, the main and subroutine processes calculate the model responses independently and simultaneously. When all the calculations are complete, the subroutine processes send the calculated results to the main process, and the main process assembles and outputs the received results. In the end, the main process finalizes the parallel environment.

The 2D parallel inversion algorithm

To test the accuracy and effectiveness of the 2D parallel forward modeling and inversion algorithm, we designed a simulation model, using a synthetic dataset. The calculations were performed on a high-performance computer with Linux operation system, Intel (R) Xeon (R) CPU E5-2620 v2 @ 2.1 GHz, and 128 GB of memory.

Synthetic dataset

In the inversion, we use multi-array electric field data to recover the four parameters of the Cole–Cole model. The setup is dipole–dipole. The transmitting source has finite length and is located in the x-direction. The length of the transmitting source is 1 m, and the current is 1 A. The length of the dipole receiver is 50 m. The five frequencies of choice are 0.1 Hz, 1.0 Hz, 8.0 Hz, 32.0 Hz, and 128.0 Hz. We used 21 transmitters 100 m apart and 40 receivers 50 m apart from X = –1000 m to X = 1000, with the exception of the location of the transmitting source. The configuration of the SIP survey is shown in Figure 5.

Figure 6 shows a 200 m long and 100 m thick anomaly. The top of the geological anomaly is 100 m beneath the surface. The center of the anomaly is at the origin ($x = y = z = 0$). The Cole–Cole model parameters of the anomalous body are DC resistivity $\rho_0 = 100$ Ω·m, chargeability $m = 0.5$, relaxation constant $c = 0.5$, and time constant $\tau = 30$ s. The resistivity of the surrounding rock is 100 Ω·m. To simulate the field data, we added 1% noise to the forward modeling data. The initial inversion model is the uniform polarization half-space, with DC resistivity $\rho_0 = 100$ Ω·m, chargeability $m = 0.01$, relaxation constant $c = 0.2$, and time constant $\tau = 10$ s. The inversion region is divided into 40 × 53 discrete elements. The misfit threshold in the inversion is 1.0.

We carry out the inversion and calculate the root mean square (RMS) as a function of the number of iterations (Figure 7). The initial RMS value is 31.2 and after three iterations the RMS decreases. When fitting the observed data, it is important to search for the smoothest model.

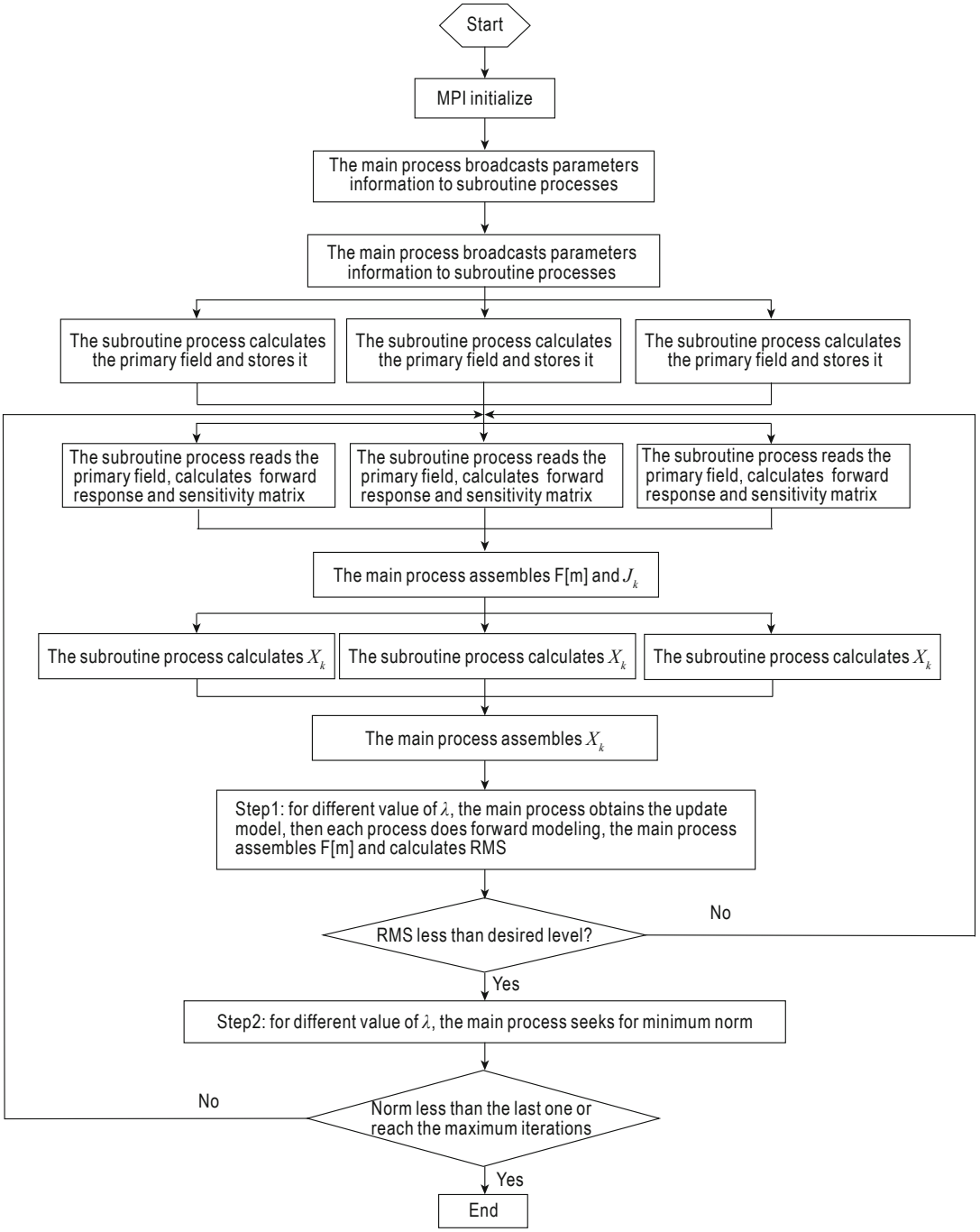

Fig.4 Flow chart of parallel inversion in data space.

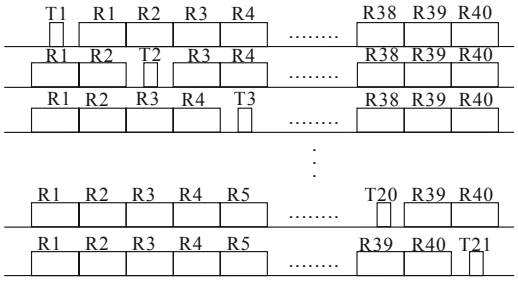

Fig.5 Configuration of the SIP survey.

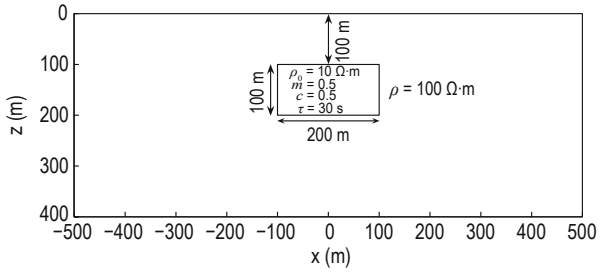

Fig.6 Diagram of low resistivity and polarization model.

The inversion results for the four parameters of the Cole–Cole model are shown in Figures 8, 9, 10, and 11, respectively. The DC resistivity, chargeability, and relaxation constant are well represented, and the location and geometry of the anomaly are clearly observed and are very close to the true values. However, the time constant, as shown in Figure 11, is poorly correlated with the true values. This is because the time constant is less sensitive than the other parameters (Loke et al., 2006). Owing to the multi-array electric field data participating in the inversion, the electric field data fitting curve of the two different transmitter sources corresponding to different receivers is shown in Figure 12. Circles "o" represent the observed data, stars "*" denote the model response generated from the sixth inversion iteration, Tx denotes the location of the transmitter source, and

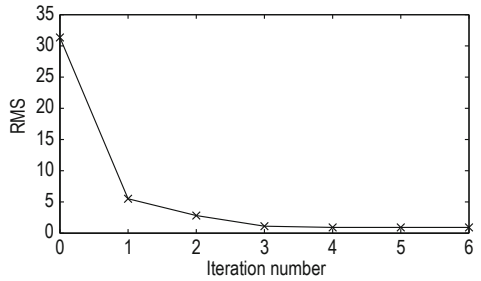

Fig.7 The RMS misfit for the inversion.

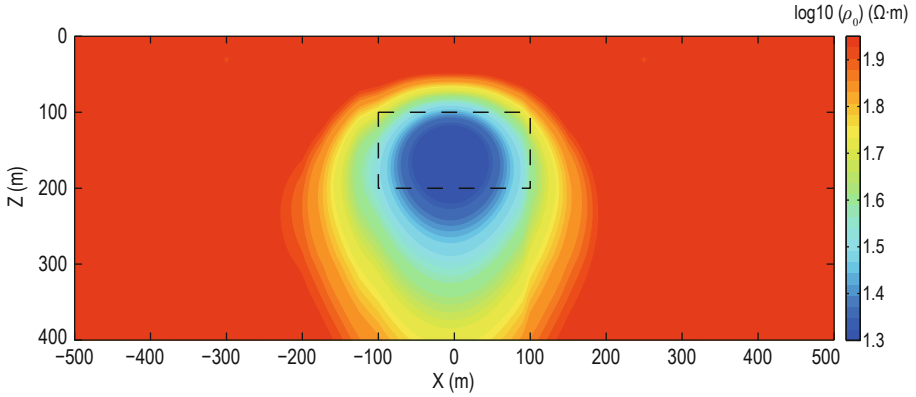

Fig.8 Inversion result of DC resistivity.

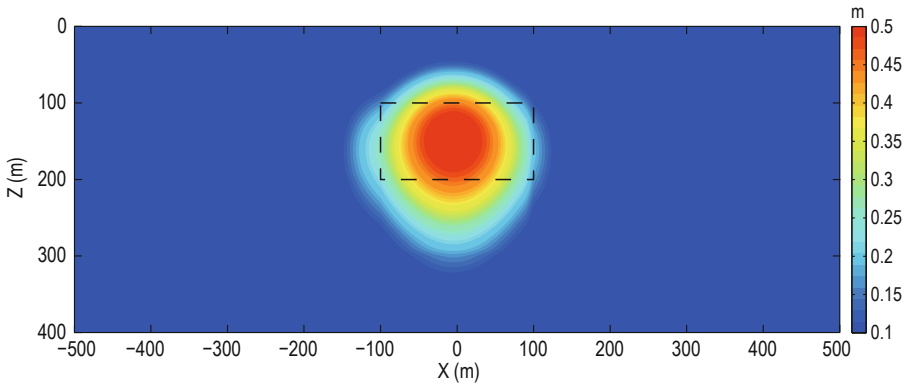

Fig.9 Inversion result of chargeability.

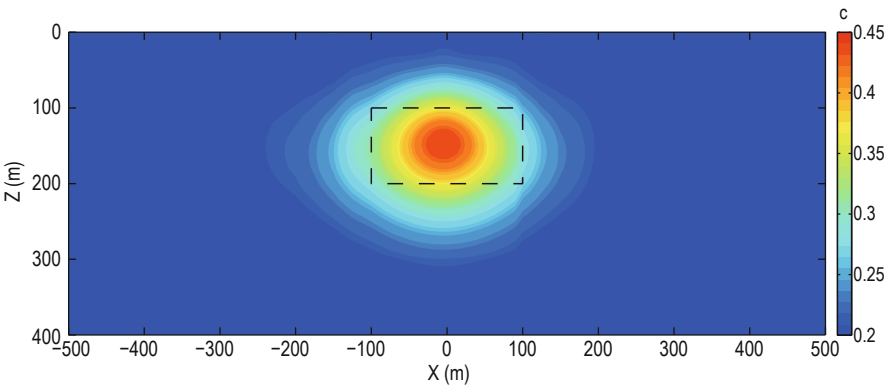

Fig.10 Inversion result of relaxation parameter.

Rx denotes the location of the receiver. We can see that the results are almost identical and the relative errors are below 0.4%.

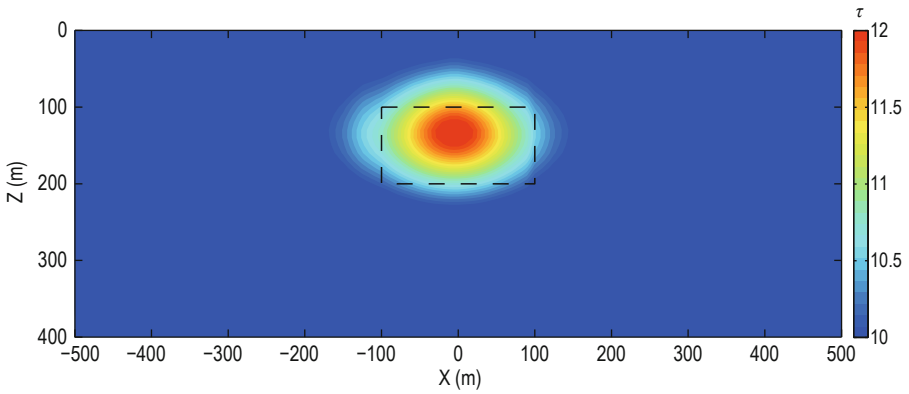

Fig.11 Inversion result of time constant.

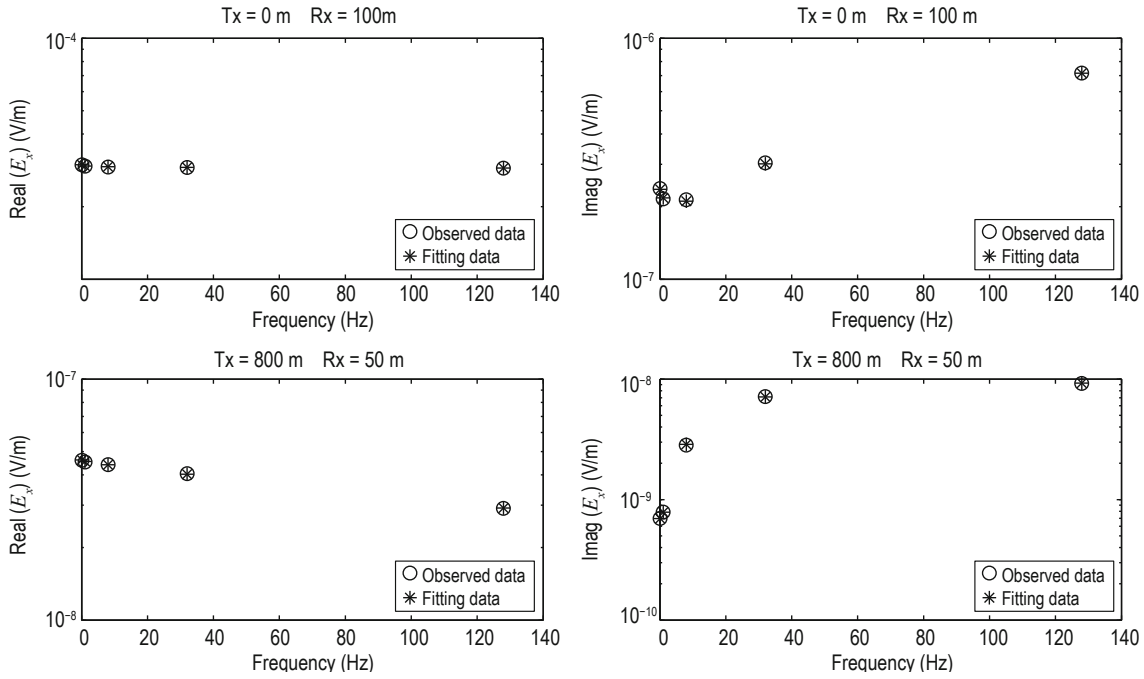

Fig.12 E_x component fitting curve.

Parallel algorithm efficiency

The parallel inversion is based on the MPI library and the DASOCC is used to invert the Cole–Cole model parameters; thus, the inversion is computer memory intensive. For example, it requires about 4 GB for five frequencies, 21 transmitter sources, and 40 receivers for each transmitter, and a model of 121 × 64 discrete blocks. Therefore, the program can be executed on a small workstation. To test the efficiency of the 2D parallel algorithm, we first invert the model and record the overall time. Different processes are then adopted to calculate the model and evaluate the effect of parallel algorithm on the speedup ratio and parallel efficiency. The speedup ratio equals the runtime of the serial algorithm divided by the runtime of the parallel algorithm. The parallel efficiency equals the speedup ratio divided by the number of processors that participate in the parallel algorithm. The runtimes of the serial and parallel inversion algorithms for the 2D model are given in Table 1.

Table 1 Statistical runtime of serial and parallel inversions for a 2D model

Running mode	Number of processes	Number of sources in each process	2D grid size	Runtimes (h)	Speed-up ratio	Parallel efficiency
Serial algorithm	1	21	121×64	121.29	none	none
Parallel algorithm	2	11,10	121×64	71.34	1.70	85%
	3	7,7,7	121×64	49.93	2.43	81%
	4	6,5,5,5	121×64	45.28	2.68	67%
	7	3,3,3,3,3,3,3	121×64	30.05	4.04	57.7%

As it can be seen from Table 1, the speedup ratio gradually increases with increasing processes. The use of MPI increases the computation efficiency and decreases the time required to carry out the inversion. However, as the number of processes increases, the parallel efficiency gradually decreases. This is because the communication between processes is time consuming and, as the number of processes increases, the communication time between processes increases. In general, the parallel program significantly improves the computation efficiency of serial algorithms and greatly reduces the time it takes to carry out the inversion.

Conclusions

We used FEM to perform 2D SIP forward modeling and then the data-space Occam method to perform 2D SIP inversion. A multi-array electric field dataset Ex is used to invert the four parameters (DC resistivity, chargeability, relaxation constant, and time constant) of the Cole–Cole model simultaneously. The use of parametric boundary constraints during inversion reduces the nonuniqueness of the inversion, and the weight of the Lagrange multiplier of each parameter generated from the ratio between each parameter's sensitivity matrix makes the inversion more stable. We use a synthetic dataset to test the validity and stability of the inversion algorithm. To improve the calculation efficiency of the inversion algorithm, we use the MPI library to perform the inversion, using different transmitting sources after thoroughly analyzing the serial algorithm. The parallel algorithm and the synthetic dataset were assessed using different numbers of processes. The comparison of the results of the parallel and serial algorithms suggests that the parallel algorithm is realistic, stable, and efficient.

References

Attwa, M., and Günther, T., 2013, Spectral induced polarization measurements for environmental purposes and predicting the hydraulic conductivity in sandy aquifers: Hydrology and Earth System Sciences Discussions, **10**(4), 5315–5354.

Avdeev, D. B., 2005, Three-dimensional electromagnetic modelling and inversion from theory to application: Surveys in Geophysics, **26**(6), 767–799.

Commer, M., and Newman, G. A., 2008, New advances in three-dimensional controlled-source electromagnetic inversion: Geophysical Journal International, **172**(2), 513 –535.

Constable, C. S., Parker, R. L., and Constable, C. G., 1987, Occam's inversion: A practical algorithm for generating a smooth models from electromagnetic sounding data: Geophysics, **52**(3), 289–300.

Egbert, G. D., Bennett, A. F., and Foreman, M. G.G., 1994, TOPEX/POSEIDON tides estimated using a global inverse model: Journal of Geophysical Research, **99**(c12), 24821–24852.

Fan, C. S., Li, T. L., and Yan, J. Y., 2012, Research and application experiment on 2.5D SIP inversion: Chinese Journal of Geophysics (in Chinese), **55**(12), 4044–4050.

Fan, C. S., 2013, Research on complex resistivity forward and inversion with finite element method and its application: PhD Thesis, Jilin University.

Kemna, A., Binley, A., Ramirez, A., and Daily, W., 2000, Complex resistivity tomography for environmental applications: Chemical Engineering Journal, **77**(1), 11–18.

Key, K., and Ovall, J., 2011, A parallel goal-oriented adaptive finite element method for 2.5-D electromagnetic modelling: Geophysical Journal International, **186**(1), 137–154.

Kim, H. J., Song, Y., and Lee, K. H., 1999, Inequality constraint in least-squares inversion of geophysical data: Earth Planets Space, **51**, 255–259.

Li, Y. G., and Key, K., 2007, 2D marine controlled-source electromagnetic modeling: Part 1 – An adaptive finite-element algorithm: Geophysics, **72**(2), WA51–WA62.

Loke, M. H., Chambers J. E., and Ogilvy., R. D., 2006, Inversion of 2D spectral induced polarization imaging data: Geophysical Prospecting, **54**(3), 287–301.

McGillivray, P. R., Oldenburg, D. W., Ellis R. G., and Habashy, T. M., 1994, Calculation of sensitivities for the frequency-domain electromagnetic problem: Geophysical Journal International, **116**(1), 1–4.

Mitsuhata, Y., 2000, 2-D electromagnetic modeling by finite-element method with a dipole source and topography: Geophysics, **65**(2), 465–475.

Nabighian, M. N., 1988, Electromagnetic Methods in Applied Geophysics, vol. 1: Theory. Society of Exploration Geophysicists.

Pacheco, P. S., 2011, An Introduction to Parallel Programming, Morgan Kaufann Publ. Inc.

Pelton, W. H., Ward, S. H., Hallof, P. G., Sill, W. R., and Nelson, P. H., 1978, Mineral discrimination and removal of inductive coupling with multifrequency IP: Geophysics, **43**(3), 588–609.

Revil, A., Karaoulis, M., Johnson, T., and Kemna., A., 2012, Review: Some low-frequency electrical methods for subsurface characterization and monitoring in hydrogeology: Hydrogeology Journal, **20**(4), 617–658.

Routh, P. S., Oldenburg, D. W., and Li, Y. G., 1998, Regularized inversion of spectral IP parameters from complex resistivity data: 68th Annual International Meeting, SEG Expanded Abstracts, 810−813.

Schwartz, N., and Furman, A., 2012, Spectral induced polarization signature of soil contaminated by organic pollutant: Experiment and modeling: Journal of Geophysical Research, **117**, B10203.

Shin, S., Park, S., and Shin, D, 2015, Spectral-induced polarization characteristics of rock types from the skarn deposit in Gagok Mine, Taebaeksan Basin, South Korea: Environmental Earth Sciences, **73**(12), 8325–8331.

Siripunvaraporn, W., and Egbert, G., 2000, An efficient data-subspace inversion method for 2-D magnetotelluric data: Geophysics, **65**(3), 791–803.

Siripunvaraporn, W., Egbert, G., Lenbury, Y., and Uyeshima, M., 2005, Three-dimensional magnetotelluric inversion: data space method: Physics of the Earth and Planetary Interiors, **150**(1–3), 3–14.

Xu, K. J., 2007, Study on 2.5D complex resistivity electromagnetic forward and inversion: PhD Thesis, Jilin University.

Yang, J., 2011, Environmental and Engineering Geophysics: Geological Publishing House, Beijing.

Zhao, G. M., 2009, Research of complex resistivity 2.5D electromagnetic forward and inversion with topography: PhD Thesis, Jilin University.

Zienkiewicz, O. C., 1977. The finite element method, McGraw-Hill Book Co.

Zhang Zhi-Yong, He received his M.S. in 2013 from China University of Geosciences, Beijing. Currently, he is a Ph.D. student at the School of Geophysics and Information Technology, China University of Geosciences, Beijing. His main research interests are electromagnetic forward modeling and inversion.